Research Article | Vol. 9, No. 9 / 1 September 2019 / Optical Materials Express 3789
Optical Materials EXPRESS

Modeling of residual tool mark formation and its influence on the optical performance of KH_2PO_4 optics repaired by micro-milling

Qi Liu,[1,2,3] Jian Cheng,[1,3,4] Hao Yang,[1] Yafei Xu,[1] Linjie Zhao,[1] Chao Tan,[1] and Mingjun Chen[1,2,5]

[1]State Key Laboratory of Robotics and System, Harbin Institute of Technology, Harbin 150001, China
[2]Center for Precision Engineering, Harbin Institute of Technology, Harbin 150001, China
[3]These authors contributed equally to this work
[4]cheng.826@hit.edu.cn
[5]chenmj@hit.edu.cn

Abstract: In the micro-milling repair process of surface defects on KH_2PO_4 (KDP) optics, residual tool marks are inevitably introduced on repaired surfaces. These tool marks could present great potential risks in lowering laser-induced damage thresholds of repaired KDP optics, which has not been reported in the previous works. In this work, the formation process of micro-milled tool marks was initially modeled and then the effect of these residual marks on the optical performance of KDP optics was investigated theoretically and experimentally. A 3D surface generation model for repair contours is proposed to predict the profiles of residual tool marks on micro ball-end milled surfaces, and then a numerical FEM model adopting the calculated profiles of residual tool marks is established to investigate the light intensification inside KDP optics based on electromagnetic theory. The relationship between repair machining processes, tool marks profiles and light intensifications as well as laser damage resistance of repaired KDP optics, has been discussed comprehensively and systematically. Practical repair experiments and laser damage tests verified the theoretical results very well. It revealed that the residual height of tool marks can induce apparent diffraction effect, consequently causing severe light intensification inside KDP optics. The micro milling strategies (e.g. a combination of layer-milling and spiral milling paths) can also exert a positive role in improving the laser damage resistance of KDP optics. An optimized repair process flow, adopting layer-milling path as rough milling and employing spiral-milling with path intervals of 10~15 μm as fine milling, is recommended for the future practical engineering repair of full-aperture KDP optics in ICF facilities.

1. Introduction

Owing to the excellent nonlinear optical and electro-optical properties, potassium dihydrogen phosphate (KH_2PO_4/KDP) crystals are currently the unique candidate for terminal frequency converters and optical switch-Pockels cells in the laser-driven inertial confinement fusion (ICF) facilities [1,2], such as the National Ignition Facility (NIF) in the USA [3] and the SG-III in China [4]. Nevertheless, some micro-defects (e.g., cracks, laser ablation) are vulnerable generated on the surfaces of KDP optics during the ultra-precision fly-cut process and high-power laser pre-irradiation because of its soft-brittle mechanical properties [5,6]. These defects can dramatically grow under the subsequent high-power laser irradiation, eventually resulting in the failure of the whole optical element [7–9]. Considering the expensive cost of crystal growth [10], it is of great significance to repair these defects for curbing the damage growth and improving the laser-induced damage threshold (LIDT) of KDP optics. During the last decades, many advanced techniques, including micro-machining, short-pulse laser ablation, water etching [11], and CO_2

#370494 https://doi.org/10.1364/OME.9.003789
Journal © 2019 Received 19 Jun 2019; revised 8 Aug 2019; accepted 8 Aug 2019; published 26 Aug 2019

Optical Materials EXPRESS

laser melting, have been employed to repair micro-defects on KDP surfaces [12]. Among them, micro-milling has been recognized as the most promising method to achieve repair tasks and can be applied in the future engineering mitigation of large-aperture KDP optics [13].

To promote the practical application of micro-milling repair technique in the construction of ICF facilities, considerable efforts have been devoted to the ductile-regime machining of KDP crystal and the optimization of repair contours. The first one mainly deals with the cutting mechanism of brittle-to-ductile transition in KDP machining process for obtaining a smooth and fracture-free surface [14–16], and the other one focuses on how to design suitable mitigation contours (e.g. Gaussian, conical and spherical pits) for various types of surface defects with the aim of ensuring the minimum loss of laser damage resistance [17,18]. However, in addition to these two aspects, there is another point that could severely affect the laser damage resistance of repaired KDP optics, which is the surface morphologies on repaired KDP surface. Actually, after micro ball-end milling process, residual tool marks, the major component of repaired surface morphologies, are inevitably generated on machined surfaces due to the geometric cutter-workpiece intersection between successive cutting paths [19]. The height of micro-milled tool marks is normally at hundreds of nanometers, which is very close to the working laser wavelength in ICF facilities. There is no doubt that these residual tool marks could exert a significant impact on the optical performance of KDP optics. But to the state of art, this issue concerning the detailed role of residual tool marks has not been realized and remains to be explored systematically.

In this respect, studying the formation mechanism of tool marks in the micro-milling process is of high importance. Chen [20] pointed out that tool marks generated in the milling process are the result of the interaction between the ball-shape cutter and workpiece when the cutter moves along successive paths separated by an offset distance (named path interval). Irene [21] revealed that the morphology of tool marks is a function of machining parameters (e.g. depth of cut, feed per tooth and path interval). Peng [22] and Li [23] further reported that machined surface textures can be controlled by inclining cutters along different feed direction. To observe the formation process of tool marks directly, Chen [24,25] has developed a surface generation model and achieved an accurate prediction of surface textures after machining. However, these previous works only considered the situation that all machined surfaces are only two-dimension planes and have not come to complex three-dimension (3D) curved surfaces. These curved surfaces normally possess varying radius of gyration or varying curvature [17]. This means when fabricating the predesigned mitigation contours, the micro ball-end milling cutter is supposed to move along more complicated trajectories rather than simple parallel linear paths [26,27]. Besides, the machining parameters would also exert a different impact on the dynamic interaction between the ball-shaped cutter and workpiece as the change of gyration radius [28]. But the knowledge of the relationship between machining factors and the generation of tool marks is still lacking when micro-milling complex curved surfaces. Thus, the formation mechanism of tool marks on repaired contours is in urgent need to optimize the micro-milling repair process of KDP optics.

For improving the laser damage resistance of KDP optics, a great deal of effort has been also made to explore the damage mechanism when they are irradiated under the high-power laser. The damage initiation and growth are found to be closely associated with light intensification, enhanced scattering and nonlinear heat absorption [29,30]. Among them, the light intensification has been identified as the primary cause of laser damage growth. Using light intensification as an evaluation index for characterizing the laser damage resistance, Cheng [6] figured out that light field intensities inside KDP optics can be modulated heavily by surfaces cracks and the modulation extent is closely dependent on laser wavelength, crack geometry and crack position. Li [31] stated that scratches can distort heavily the local optical fields of incident laser, and consequently reduce the LIDT of KDP optics by more than 30%. One can see that any structure

Optical Materials EXPRESS

change on KDP original surfaces could exert a direct impact on its internal light field intensity. In our previous works, we have designed and optimized repair contours for different types of surface cracks to effectively improve LIDTs of repaired KDP optics [17,32]. Larger width-to-depth ratio (more than 5) is recommended for each type of contours because this size can avoid the occurrence of total reflection effect and is beneficial to reduce the light intensification. But these works just regarded the micro-milled contours as ideally smooth surfaces and ignored the existence of residual tool marks. Hence, taking a thorough investigation on the influence of residual tool marks on laser damage resistance can not only enhance our understanding of laser damage mechanisms but also provides instructive guidance for the practical repairing process of full-aperture KDP optics.

To fill the gap mentioned above, the effect of residual tool marks on the optical performance of micro-milled KDP optics was investigated in this work. Firstly, a 3D surface generation model for repair contours is developed to acquire the residual tool marks profiles on repaired surfaces. Then, adopting these calculated tool marks profiles, a numerical model based on electromagnetic theory is proposed to simulate the light intensification induced by tool marks using the finite element method (FEM). Further, the relationship between repair machining process, tool marks morphology and light intensification has been discussed comprehensively and systematically. Finally, practical repair experiments and corresponding laser damage tests have been carried out. The experimental results agree well with the simulation results and an optimization micro-milling repair process is recommended for enhancing the laser damage resistance of KDP optics.

2. Material and experiments

2.1. Fabrication of conical mitigation pits on KDP optics

A homebuilt multi-axis repairing machine tool has been developed. This equipment can achieve some specific functions for the repairing process of KDP surface defects, including fast defect identification, repairing monitoring, precision tool pre-setting and micro-milling repairing. Figure 1 shows the micro-milling system for the repair of micro-defects. A high-speed motorized spindle (BMJ-320, NAKANISHI) used in this machine can achieve a maximum speed of 80,000 RPM. The moving stage is linear motion units, which can achieve the resolution of 0.01 μm, 0.01 μm and 0.05μm along X, Y, Z axis, respectively. After fabricated by fly-cutting, a KDP crystal bulk with a dimension of $50 \times 50 \times 10$ mm was employed as the workpiece. A cubic boron nitride micro ball-end milling cutter with a radius of 0.25 mm was utilized in the repairing experiments (SSBL 200, NS Tool). This micro-milling cutter has two cutting edges and possesses a helix angle of zero degrees. Meanwhile, the spindle was tilted with an angle of 45° to the horizontal level.

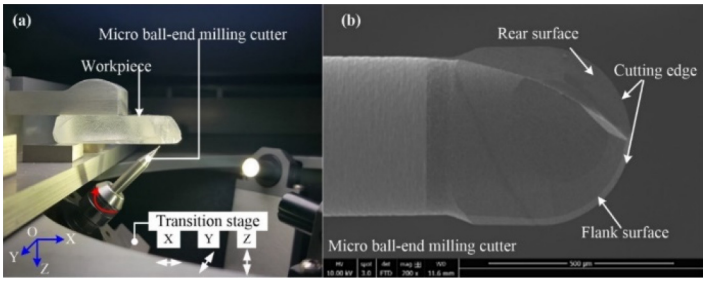

Fig. 1. Images of machining equipment: (a) the micro-milling sub-system; (b) the micro ball-end milling cutter.

In the current study of repairing KDP optics, the layer-milling is adopted as the general way to transfer micro-defects to smooth contours, but the machined surface quality is not pretty good.

Optical Materials EXPRESS

Thus, to better improve the optical performance of repaired KDP optics, an optimal milling approach is proposed in this work, combining the layer-milling and spiral-milling process. The essential difference between these two kinds of milling strategies is the trajectory of the cutter in micro-milling process. In the layer-milling process, the damaged material is normally removed by layer-by-layer, while in the spiral-milling process the cutter can fabricate the predesigned contours along a spiral trajectory with a constant path interval. How milling strategies influence the surface morphology is also the primary purpose of this work and will be discussed later. The path interval used in the layer-milling process was set as 40 μm as it can not only improve the machining efficiency but also guarantee the ductile-regime machining. While in spiral-milling process, the path interval was set from 5 μm to 30 μm (in steps of 5 μm). The depth of cut was set as 1μm as this is the allowed minimum value due to the ploughing effect [33], indicating that the repaired surface quality using the depth of cut of 1μm is close to the best surface quality at the same milling condition. The spindle speed and feed rate were set as 50,000 RPM and 1.2 mm/s, respectively, as listed in Table 1. Owing to the soft-brittle property of KDP crystals, brittle-regime machining could be easily caused by even very small cutting forces, causing cracks or fracture left on the machined surfaces. One of our previous research [15] has revealed that the undeformed chip thickness plays a vital role in the brittle-to-ductile transition and stated that the machining parameters should be selected carefully when micro-milling KDP crystals. All of these parameters have been proved to benefit the ductile-regime machining of KDP crystal, and can be referred in Ref. [34,35].

Table 1. Parameters applied in micro-milling mitigation contours on KDP surfaces.

Parameters	Values
Cutter radius R (μm)	250
Milling strategy	Layer-milling; Spiral milling
Feed rate f (mm/min)	48
Cutting depth ap (μm)	0.1
Spindle speed n (RPM)	50000
Spindle inclining angle (°)	45
Path intervals (μm)	Layer-milling: 40
	Spiral-milling:5,10,15,20,25,30

The morphology of repaired pits was observed by white light interferometer (Newview 8200, Zygo), which can also be used to measure the surface roughness. The morphology of tool marks was observed by AFM (Dimension 3100, Veeco) and SEM (JCM-5000, JEOL). Benefitting from the nanoscale resolution of AFM, the residual tool marks height can be accurately acquired. For each repaired contour, the surface roughness and residual tool marks height are the average value in five times tests.

2.2. Test of the optical performance of micro-milled KDP optics

The influence of various tool marks on the optical performance of repaired KDP optics can be evaluated by the optical transmittance capacity and laser damage resistance through laser irradiation experiments. Conical mitigation contours were firstly fabricated using various path intervals listed in Table 1. For each path intervals, a total of 10 test sites were produced. Then, the optical transmittance of these samples was tested via Lambda 950 spectrophotometer, which can measure the transmittance of optics at wavelengths from 900 nm to 1200 nm. After irradiation, the transmittance at 1064 nm wavelength was picked up and estimated as the average values to qualitatively validate the calculated light intensification induced by various tool marks.

Optical Materials EXPRESS

The laser damage test was also carried out to measure the LIDTs and to evaluate the laser damage resistance of repaired KDP optics with different tool marks. Figure 2 illustrates the schematic of the laser damage test system, which consists of the Nd: YAG lasers, high precision translation stage, and laser focusing lens, etc. The intense pulsed lasers used in tests worked at the wavelength 1064 nm, the pulse duration 10 ns and the pulse repetition frequency 1 Hz. The laser normally irradiated on repaired KDP mitigation contours, which was mounted on the 3-axis transition stage. In addition, an in-situ CCD camera was employed to monitor the morphology evolution of sample surfaces. The R-on-1 [7] protocol was adopted in this work, and for each kind of repaired surfaces, a total of 10 test sites were irradiated with laser fluence ramping up until the damage takes place. The LIDT is estimated as the average value of the lowest fluence corresponding to the initiation of laser damage. More experimental details can be found in Refs. [32,36].

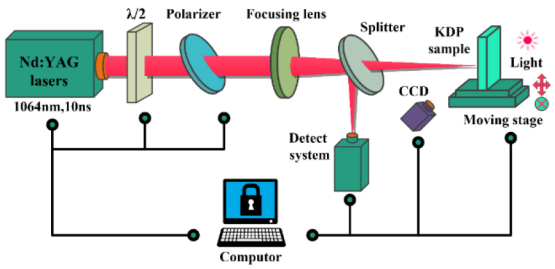

Fig. 2. Schematic of the laser system designed to test the LIDTs of micro-milled KDP surfaces [36].

3. Modeling of repaired contour formation and residual tool marks

3.1. Characterization of tool marks on micro-milled conical contours

Figure 3 illustrates the schematic of micro ball-end milling repair processes of surface defects on KDP optics. One can see that a micro ball-end milling cutter could remove surface defects along predesigned paths, and then transfer them into predesigned contours like conical contours. But due to the geometric tool-workpiece intersection between successive cutting paths (O_i and O_{i+1}), a shaded area ABC, named residual tool mark, will be inevitable left on the machined surface. These tool marks normally possess a residual height of several hundred nanometers which is very close to the working laser wavelength in ICF facilities. Therefore, these periodical surface micro-structures must exert a direct role in the light propagation once the repaired KDP optics are irradiated by the high-power laser.

To clarify it better, Fig. 4 displays the morphology of practically repaired conical contours and corresponding residual tool marks. One can see that residual tool marks on conical contour surfaces are clearly visible and mainly distribute perpendicular with the feed direction. In contrast, the residual tool marks along feed direction are so small that their impact on the laser damage resistance of KDP optics can be ignored [37]. Similarly, the high-frequency features on the repaired surfaces, as shown in Fig. 4(b) should also be neglected in this work. Meanwhile, the period of these tool marks is approximately equal to path interval (15 um) used in the spiral-milling process. The section profile, as shown in Fig. 4(d), verifies that the formation of tool marks is due to the overlapping of adjacent two ball-end shape milling cutter. The above experimental results can effectively verify the existence of residual tool marks and indicate that the influence of tool marks cannot be ignored when analyzing the surface quality as well as the optical performance of repaired KDP crystal.

Optical Materials EXPRESS

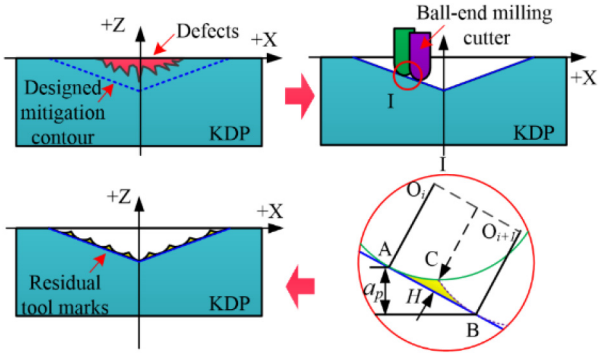

Fig. 3. Schematic of the generation process of tool marks in the micro ball-end milling repair process of KDP optics.

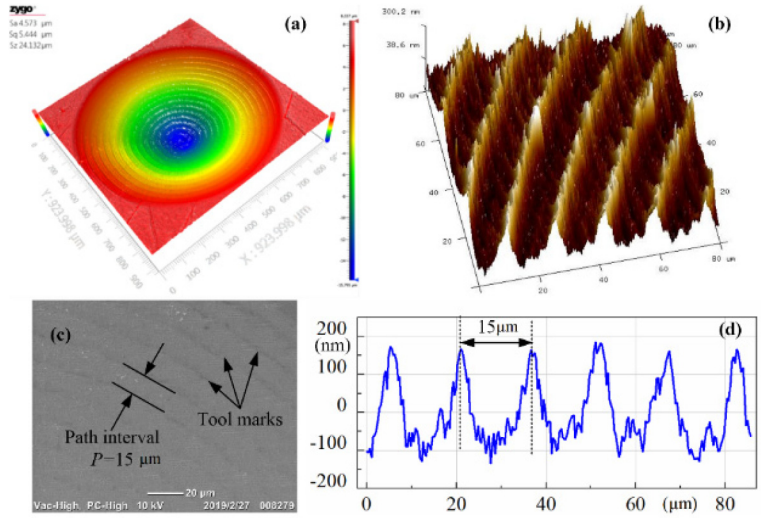

Fig. 4. Morphologies of repaired conical contour measured by optical profiler (a) and tool marks measured by AFM (b) an SEM (c). (d) is the cross-section profile of tool marks extracted from (b).

Optical Materials EXPRESS

3.2. Surface generation modeling in micro-milling conical contours

With the aim to accurately predict the morphology of residual tool marks, one calculation algorithm based on homogeneous matrix transformation (HMT) was developed to predict the surface morphology of conical pit after machining. And it mainly consists of the following steps: Firstly, the cutting edge is discretized into a series of points and is described with a numerical function. Secondly, the dynamic function of all discretized points on the cutting is also established based on the HMT. Finally, the Z-Map method considering various milling trajectories is applied to predict the final machined surface.

3.2.1. Cutting edge modeling and the homogeneous matrix transformation

To obtain the surface topography of the repaired workpiece, a spherical coordinate system is first established. The geometry of the ball-end milling tool and corresponding cutting edges is present in Fig. 5. The cutter spherical center O is defined as the origin point of $X_cY_cZ_c$ tool coordinate system. For any point P_i, its position can be expressed by two parameters: (i) included angle α between line OP_i and OX axis; (ii) included angle β between OP_i and OZ axis; Therefore, the coordinate function of point P_i can be expressed as

$$\begin{cases} x_i = R_i \cdot \sin\beta_i \cdot \cos\alpha_i \\ y_i = R_i \cdot \sin\beta_i \cdot \sin\alpha_i \\ z_i = -R_i \cdot \cos\beta_i \end{cases} \tag{1}$$

In the micro-milling process, the movement of cutting edge is dynamic, consisting of the rotation around the cutter axis and the translation with the cutter. The rotation movement will change the phase angle α of point P_i while the translation movement will change the relative position of P_i to global coordinate, as shown in Fig. 5(c) and (d). Assume the ball-end milling cutter moves along a specific path from location A (x_0, y_0, z_0) to location B (x_t, y_t, z_t), the coordinate of infinitesimal point P_i relative to the workpiece coordinate can be described as:

$$\begin{Bmatrix} x_t \\ y_t \\ z_t \\ 1 \end{Bmatrix} = \begin{Bmatrix} 1 & & & f_x t \\ & 1 & & f_y t \\ & & 1 & f_z t \\ & & & 1 \end{Bmatrix} \begin{Bmatrix} x_0 \\ y_0 \\ z_0 \\ 1 \end{Bmatrix} + \begin{Bmatrix} R \cdot \sin\beta \cdot \cos\alpha_i \\ R \cdot \sin\beta \cdot \cos\alpha_i \\ -R \cdot \cos\beta \\ 1 \end{Bmatrix} \tag{2}$$

where f_x, f_y, f_z denote the components of feed rate along with different coordinate directions.

The top-point of ball-end milling cutter possess a zero-cutting speed and could damage the machined surface quality [34]. Thus, tilting the tool-axis with an inclination angle relative to the normal direction of the machined surface is a usual method to avoid cutter top-point engaging

Optical Materials EXPRESS

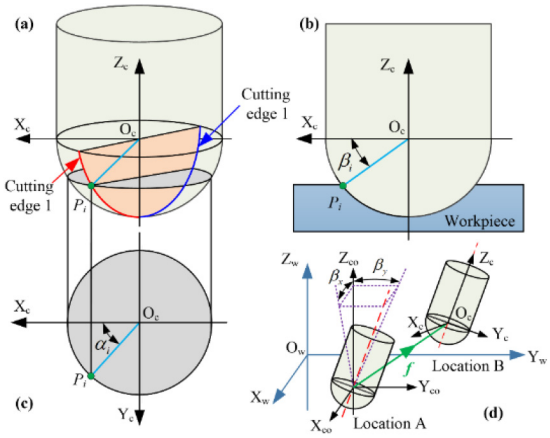

Fig. 5. Illustration of ball-end milling cutter geometry (a)–(c) and the cutter movement in the workpiece coordinate system.

into cutting. Once the tool-axis is tilted, the coordinate will become as

$$\begin{Bmatrix} x_t \\ y_t \\ z_t \\ 1 \end{Bmatrix} = \begin{Bmatrix} 1 & & & f_x t \\ & 1 & & f_y t \\ & & 1 & f_z t \\ & & & 1 \end{Bmatrix} \begin{Bmatrix} x_0 \\ y_0 \\ z_0 \\ 1 \end{Bmatrix} + \begin{Bmatrix} 1 & & & \\ & \cos\beta_x & -\sin\beta_y & \\ & \sin\beta_x & \cos\beta_x & \\ & & & 1 \end{Bmatrix} \begin{Bmatrix} \cos\beta_y & & \sin\beta_y & \\ & 1 & & \\ \sin\beta_y & & \cos\beta_y & \\ & & & 1 \end{Bmatrix} \begin{Bmatrix} R\cdot\sin\beta\cdot\cos\alpha_i \\ R\cdot\sin\beta\cdot\cos\alpha_i \\ -R\cdot\cos\beta \\ 1 \end{Bmatrix} \tag{3}$$

where β_x, β_y are the inclination angles of the cutter relative to the original coordinate system $X_{co}Y_{co}Z_{co}$.

The Eq. (3) is the dynamic function of the cutting edge for a ball-end milling cutter in micro-milling process.

3.2.2. Surface generation simulation

As mentioned above, layer-milling and spiral-milling paths are used as main milling strategies to repair KDP optics in this work. Figure 6 displays the schematics of layer-milling and spiral-milling strategies, respectively. In layer-milling process, a layer-by-layer milling path is adopted to remove the damaged KDP material as shown in Fig. 6(a). That is to say, at the same depth of repaired pits, the cutter will feed along a concentric circle path by increasing the gyration radius with a step of 40 μm, and when this cutter reaches the contour boundary, it will go down to the next layer with a depth of cut of 1 μm and continue to feed along concentric circular paths. It can be found that residual tool marks are generated at the contour boundary by the geometric tool-workpiece intersection between adjacent layers rather than adjacent paths. This is because, for all tool marks on each layer, only the outermost tool marks will be retained and the other inner tool marks will be removed during the next layer milling process. Thus, the formation of residual tool marks is dependent on the thickness of each layer and has no relationship with path interval.

Optical Materials EXPRESS

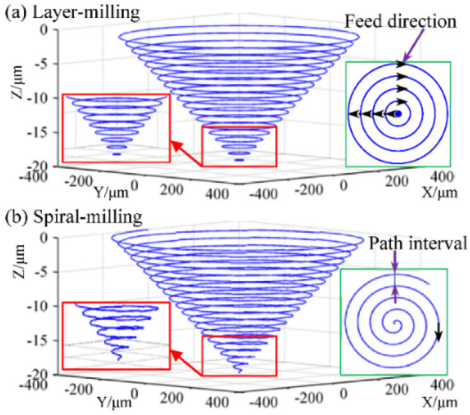

Fig. 6. The milling path in layer-milling (a) and spiral-milling process (b).

While in the spiral-milling process, a spiral milling path is adopted to fabricate the aimed contours with a constant path interval. As shown in Fig. 6(b), the cutter starts milling process at the bottom of the aimed contours and then gradually goes up along the spiral trajectory. One can see that residual tool marks are generated by the geometric intersection between adjacent milling paths. Therefore, as opposed to layer-milling process, the path interval would have a vital influence in the formation of residual tool marks in spiral-milling process.

These milling paths can be generated based on Computer Aided Manufacturing (CAM) software and the corresponding manufacturing codes can also be easily acquired. The diameter and depth of these conical contours are 800μm and 20μm, respectively. The Z-Map method is employed to generate the final machined surface [25]. This method is to plot the minimum Z as a function of X- and Y-coordinate in the workpiece coordinate system. The simulation accuracy (Δs), indicating the resolution of simulated results, is set as 0.1 μm. This value (Δs) ought to be less than the calculation accuracy (Δf) which denotes the discrete resolution of cutting edges. That is to say, the Δs should satisfy the following condition:

$$\begin{cases} \triangle s \geq (R\omega + f) \cdot \triangle t \\ \triangle s \geq R \triangle \beta \end{cases} \tag{4}$$

The parameters used in the simulation are listed in Table 1. Substituting these parameters in Eq. (4), the time discrete resolution is calculated to be less than 1×10^{-9} s and the discrete arc length less than 4×10^{-3} rad.

After calculation, the next step is to analyze the simulation data and calculate the residual height of tool marks and surface roughness. As shown in Fig. 7, point A is one peak of calculated tool marks profiles and line BC denotes the section profile of ideal conical mitigation contour. The angle γ is inclining angle of conical contours. Thus, the residual height of tool marks can be estimated as the difference between the peak of whole tool marks and the ideal surface, expressed by the following equation:

$$h = \overline{AC} = \overline{AB_{\max}} \sin(\gamma) \tag{5}$$

And the surface roughness is referred to the arithmetic average value of tool marks profile determined from deviations about ideal mitigation contour within the evaluation length. And it can be expressed as:

$$R_a = \frac{1}{l} \int_0^l A_i B_i dx \tag{6}$$

Optical Materials EXPRESS

where A_iB_i denotes the difference between tool marks and ideal mitigation contour.

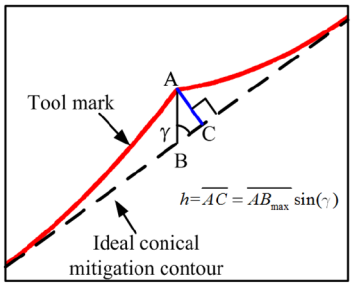

Fig. 7. Illustration of the calculation of tool marks on micro-milled mitigation contours.

4. Light intensification simulation induced by residual tool marks

Once the practical repair contours are acquired, the calculated results can be employed to build the actual profiles of residual tool marks for simulating the light modulation inside micro-milled KDP optics. Because the laser-induced damage of KDP is a complex process, which involves the anisotropy of KDP and the nonlinear heat absorption, it is very challenging to precisely simulate the damage process of KDP optics caused by residual tool marks and to build their theoretical relationship. Thus, some assumptions are made in this work: the KDP crystal is homogeneous and isotropic; the heat absorption during laser irradiation is ignored in the following simulation. Besides, the light intensification inside KDP is used to characterize the laser damage resistance of repaired KDP optics with various tool marks.

The model design and calculating details considering different tool marks morphologies are shown in Fig. 8. The light intensity modulation can be solved by Finite Element Method (FEM). As the light is a specific kind of electromagnetic wave, the propagation of laser can be regarded as the irradiation process of an electromagnetic wave, which conforms to the rigorous electromagnetic field theory. Because the electric field intensity has a functional relationship with light intensity, the electric field intensification induced by various residual tool marks is theoretically investigated. The nonhomogeneous vector wave equation of the electric field can be expressed by [29]:

$$\nabla \times (\nabla \times \mathrm{E}) - \kappa^2 \varepsilon_r \mathrm{E} = 0 \tag{7}$$

where ∇ is the differential operator, E, κ and ϵ_c denote electric field intensity, wave number and relative dielectric constant, respectively.

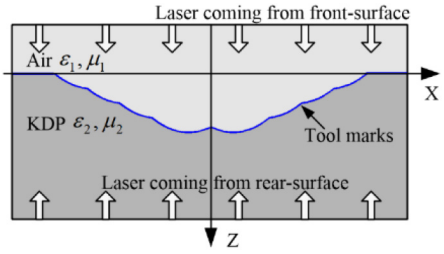

Fig. 8. The schematic of the FEM model for simulating the EM fields caused by residual tool marks on micro-milled mitigation contours

Optical Materials EXPRESS

As shown in Fig. 8, the laser incident direction is parallel to Z-axis. Thus, the component (E_z) of Eq. (7) in the Z-axis direction can be described as:

$$\frac{\partial}{\partial_x}\left(\frac{1}{\mu_r}\frac{\partial E_z}{\partial_x}\right)+\frac{\partial}{\partial y}\left(\frac{1}{\mu_r}\frac{\partial E_z}{\partial_y}\right)+k_0^2\varepsilon_r E_z=0 \tag{8}$$

where $k_0=\omega\sqrt{\varepsilon_0\mu_0}$ denotes the free-space wavenumber.

A time-harmonic plane electromagnetic wave with TE model was adopted as the incident laser and its electric field intensity was normalized as 1 V/m. A scattering boundary condition (SBC) is applied in the laser coming- and outgoing-boundary while a perfect magnetic conductor (PMC) is adopted for the boundaries which are parallel to the laser propagation direction. A reasonable meshing for the calculated domain can greatly improve the solution accuracy and save the calculation time. In this work, a free triangle mesh with two sizes of grids was adopted. Refine grids with a maximum dimension of 20 nm were employed to divide the domain in the vicinity of residual tool marks, and slightly bigger but no more than 50 nm grids were used in the other area to enhance the calculation efficiency. Meanwhile, under the incident wave of 1064 nm, the relative dielectric constant ϵ_r is 1.49, the corresponding electric conductivity σ and relative magnetic permeability μ_r are 0 and 1.0, respectively. The detailed parameters used in the simulation process are listed in Table 2.

Table 2. Parameters applied in light intensification simulation models.

wave length (w)	relative dielectric constant (ϵ_r)	electric conductivity (σ)	relative magnetic permeability (μ_r)
1064 nm	1.49	0.0	1.0

The light intensity inside optics is given by [38]:

$$I=\frac{1}{2}RE[E\times H^*]=\frac{1}{2}\sqrt{\frac{\varepsilon}{\mu}}|E|^2 \tag{9}$$

where $|E/H|$ is equal to $\sqrt{\mu/\varepsilon}$ for a time-harmonic plane electromagnetic wave.

From Eq. (9), one can see the light intensity is clearly proportional to the square of the electrical field ($|E|^2$). As mentioned above, the light intensification has been found to be closely related to the laser-induced damage growth of KDP crystals and other optics [29]. Once the light intensification exceeds a critical value, impact ionization and photon-ionization would take place. The thermal absorption of free electrons could also enhance the deterioration of the laser transmission of KDP optics [6]. Therefore, we introduced the maximum relative light intensity modulation (I_{Rmax}) here to characterize the laser damage resistance of repaired KDP optics with various tool marks:

$$I_{R\max}=\frac{I_{\max}}{I_0} \tag{10}$$

where I_0 is the ideal light intensity inside the original KDP crystal with no tool marks, and I_{Rmax} is the maximum light intensity inside KDP crystal modulated by residual tool marks. It is clear to understand that the larger I_{Rmax} is, the more probably to suffer from laser damage the KDP optics are.

To verify the accuracy and feasibility of the built FEM model, the light intensity I_0 inside flat KDP surface with no tool marks was calculated. It is found that the calculated $I_0=1.2759\times10^{-3}$ W/m^2 is very close to the theoretical one $I_{\mathrm{theo}}=1.2756\times10^{-3}$ W/m^2 according to the theory of Fresnel reflections [39], proving the proposed method is accurate and reasonable.

Optical Materials EXPRESS

5. Results and discussions

5.1. The simulation results of repaired contours and tool mark profiles

The surface simulation was carried out based on Matlab using the parameters listed in Table 1. Figure 9 displays the simulation results of conical contours (width: 800 μm×height: 20 μm) adopting layer-milling and spiral-milling paths, respectively. Because the inclined angle (γ) of conical pits keeps the same with the change of contour height, only the bottoms (width: 200 μm×height: 5 μm) of conical pits were exhibited. One can see that the surface contour adopting spiral-milling path is smoother than that adopting layer-milling path. And the simulated tool marks profiles can be acquired by extracting the cross-section contour on X-Z surface. As shown in Fig. 9(c), the fluctuations of residual tool marks on the spiral-milled surface is slight than that on the layer-milled surfaces with 10 μm path interval. Thus, the spiral-milling process has a more powerful ability than layer-milling to produce slightly tool marks with lower residual height. This indicates that the spiral-milled surfaces may have a better optical performance than layer-milled surfaces, which will be discussed in next section. It is interesting to find that although the designed depth for every mitigation contour is 20 μm, the practical machined depth in the layer-milling process is less than 20 μm. This is because the circle milling path cannot be formed at the bottom of conical contours in the layer-milling process due to the narrow workspace. In addition, the cutter moving along a smaller circle path can fabricate a salient point at the contour bottom, as shown in Fig. 9(c). This salient point can be removed if the cutter moves with a zero radius by only feeding in Z-axis direction. But there is no need to perform this step as it has no positive effect on decreasing tool marks residual height at both sides of the repaired contours. Meanwhile, this salient point and the other residual tool marks could be amended by an optimal repair process proposed in Section 5.3, adopting layer-milling path as rough-finish milling and employing spiral-milling as fine-finish milling. Anyway, the spiral-milled contour is closer to the predesigned conical contours when comparing with the layer-milled one.

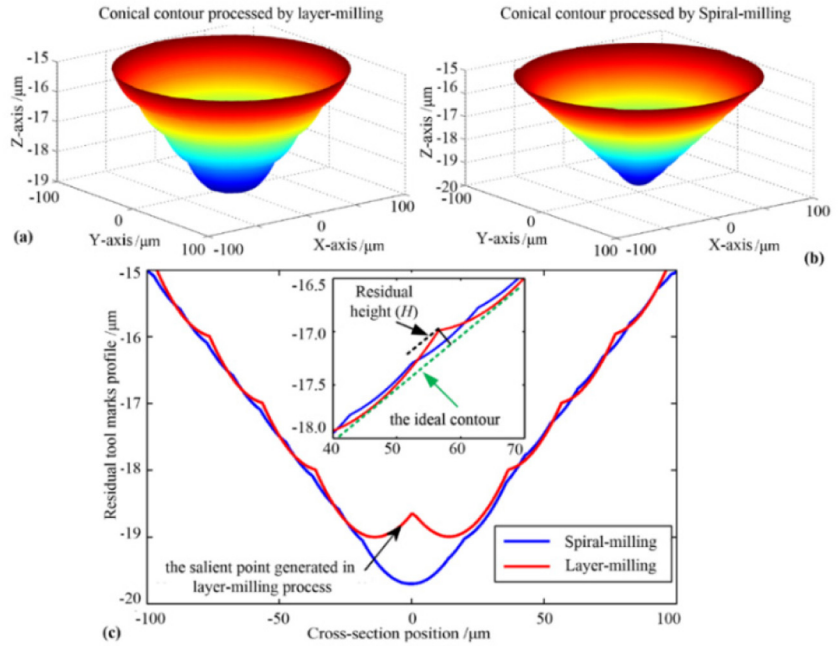

Fig. 9. Simulation results of conical mitigation contours processed by layer-milling (a) and spiral-milling (b), respectively. (c) shows the tool marks profiles extracted from (a) and (b).

Optical Materials EXPRESS

Meanwhile, the practical repairing experiments were also carried out using the same parameters (width: 800 μm× height: 20 μm). The AFM and white light interference were utilized to measure the machined surface morphologies and quality. Figure 10 shows the simulation results and experimental results in terms of surface roughness (R_a) and residual height (H). One can see that no matter for R_a or H, the simulation values and measured values agree well with each other. This means that the calculation Eqs. (5) and (6) of R_a and H are all accurate enough to evaluate the simulated results. Only a tiny discrepancy occurs in spiral-milling process at small path intervals (P = 5 μm), which may be caused by the plowing effect when the undeformed cutting depth is very small [14]. Thus, it can be emphasized that the simulation values are well consistent with the experimental results in the parameter domains in this work. In addition, as shown in Fig. 10(b)–(c), the morphology of simulated tool marks coincides well with that of measured one, evidencing the accuracy and rationality of the proposed surface simulation model.

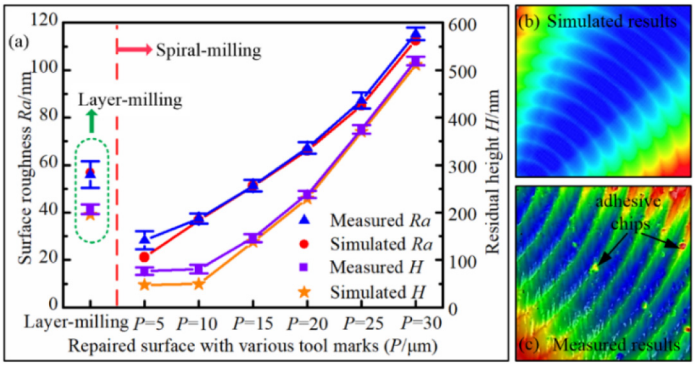

Fig. 10. The comparison of simulation and experiments results: (a) surface roughness (R_a) and residual height of tool marks (H); (b) the simulated tool marks morphology; (c) the measured tool marks morphology.

5.2. *Light intensification induced by residual tool marks*

5.2.1. Light intensification caused by spiral-milled tool marks

To investigate the influence of tool marks on the optical performance of spiral-milled KDP optics, the simulated tool marks profiles were adopted in the proposed FEM model to calculate the light intensity modulation inside KDP optics. The path intervals used in the simulation process were set from 5 μm to 30 μm in a step of 5 μm.

Figure 11 shows the evolution of I_{Rmax} induced by residual tool marks with respect to various path intervals on front- and rear-surfaces, respectively. As for the front surface processed by spiral-milling, the light intensification (I_{Rmax}) witnesses a slight decrease when the path intervals were at small values, reaching to the minimum at a path interval of 10 μm. Then there is a sharp upward trend in the I_{Rmax} with the increase of path intervals, peaking at 30 μm path interval (I_{Rmax} = 1.48). Meanwhile, a similar trend is found in the evolution of I_{Rmax} with respect to residual tool marks on rear-surface, but it is necessary to note that the I_{Rmax} caused by rear-surface tool marks is higher than that caused by front-surface tool marks for all path intervals. Besides, the I_{Rmax} for layer-milled surfaces is quite different from that for spiral-milled surface, which will be discussed in the next section.

Figure 12 shows the light intensity distributions inside KDP optics in case of tool marks with 10 μm and 30 μm path intervals. One can see that because of the modulation of tool marks, some light intensifications take place inside optics, causing the original uniform-distributed light field distorted severely. Taking front-surface tool marks with a path interval of 30 μm

Optical Materials EXPRESS

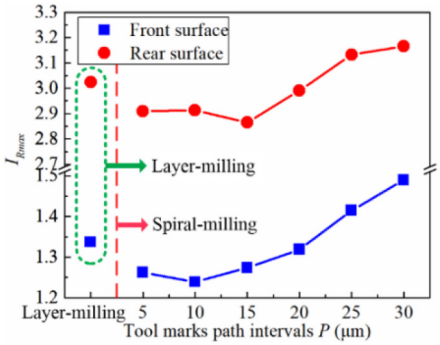

Fig. 11. The calculated light intensification I_{Rmax} induced by tool marks generated in different milling strategies. The path intervals used in the spiral-milling process are in the range from 5 μm to 30 μm in the step of 5 μm.

for instance, strong light intensifications, up to around 1.5 times, take place right beneath the peak point of residual tool marks, indicating that the corresponding spiral-milled surfaces are at higher risk of being damaged. Some diffraction ripples are clearly visible, which are formed by cross distribution between the light-enhanced regions and weakened regions, as shown in Fig. 12(c). It means that the diffraction effect is the primary cause for the light intensification inside micro-milled KDP surfaces [40]. As for the rear-surface under the same path interval, the induced I_{Rmax} is 3.2 times than the original surface with no tool marks. As can be seen from Fig. 12(d), destructive interference has been resulted from the interaction between the incident wave and reflected wave, causing higher I_{Rmax} around the rear-surface tool marks. This finding can quietly explain why the rear surfaces of KDP optics are more vulnerable to be damaged than the front surface in the practical operation of ICF facilities [6].

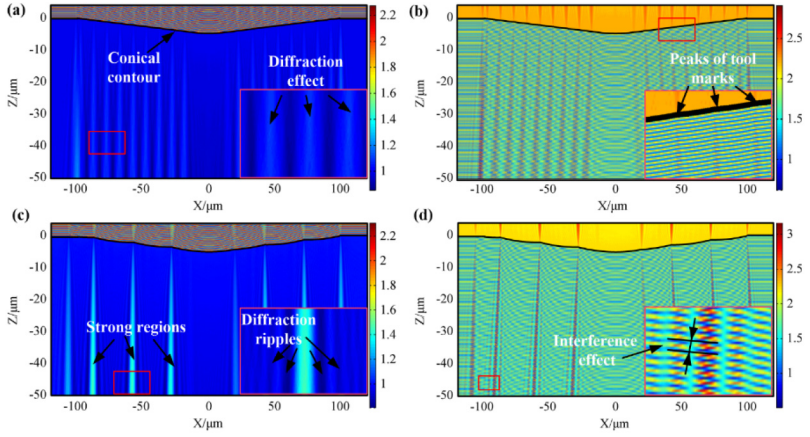

Fig. 12. The internal distributions of light intensity modulation induced by spiral-milled tool marks with path intervals of 10 μm (a, b) and 30 μm (c, d). (a) and (c)is in case of tool marks on KDP front-surface; (b) and (d) are in case of tool marks on KDP rear-surface.

When it comes to tool marks with a path interval of 10 μm, no matter for front-surface or rear surface, the induced light intensification is quite slightly. This scenario is attributed to the smaller residual height (less than 100 nm), as shown in Fig. 10. Besides, these I_{Rmax} values are also slightly lower than that related to the path interval of 5 μm. Two factors are responsible for the occurrence of relative stronger light intensification with respect to path interval of 5 μm.

Optical Materials EXPRESS

One is due to the slightly higher residual height at 5 μm, as mentioned above. The other one is that with the decrease of path interval, the diffracted ripples induced by adjacent two marks could interfere with each other, further enhancing the light intensity [18]. Thus, based on the simulation results, the path intervals in the range from 10 to 15 um are beneficial to reduce the light intensification for spiral milling process of KDP optics.

5.2.2. Difference in light intensification induced by spiral- and layer-milled tool marks

To compare the effect of various milling paths on the optical performance of the repaired optics, the light intensification induced by layer-milled tool marks were also calculated. As shown in Fig. 11, it is interesting to find that the light intensification related to layer-milled tool marks is quite different from that related to spiral-milled ones. On the one hand, the I_{Rmax} induced by layer-milled tool marks is higher than that induced by spiral-milled tool marks with periods of 5-15 μm. On the other hand, this value is lower than that with periods of 20-30 μm. In other words, the I_{Rmax} induced by layer-milled tool marks approximately equals with those induced by spiral-milling with 15-20 μm. This is because the residual height generated in layer-milling process is approximately equivalent to those generated in spiral-milling with 15-20 μm path interval, as shown in Fig. 10(a). The similar relationship also exists in the I_{Rmax} values induced by rear-surface tool marks. Therefore, it can be concluded that the induced light intensification is quite dependent on the residual height of tool marks.

When it comes to the modulation patterns, the distorted light field induced by layer-milled tool marks is also different from that induced by spiral-milled tool marks. Figure 13 shows the light intensification distribution inside repaired KDP optics by the layer-milling process. One can see that the maximum I_{Rmax} occurs beneath the bottom of conical contours. This scenario is attributed to the salient point produced by the layer-milling process. As shown in Fig. 9(c), the residual height of this salient point is much larger than that of other points on this tool mark profile [41], meaning that a more severe diffraction effect could take place in this area. In other words, the bottom of layer-milled contours is more susceptive to be damaged when they are irradiated by a high-power laser.

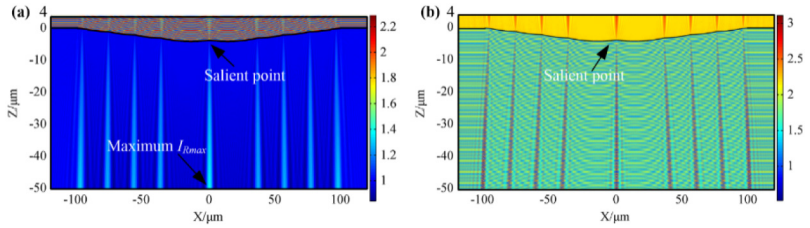

Fig. 13. The internal distributions of light intensity modulation induced by layer-milled tool marks: (a) tool marks on KDP front-surface; (b) tool marks on KDP rear-surface.

5.3. *Test of optical transmittance and laser damage of micro-milled KDP surfaces*

Figure 14 illuminates the measured optical transmittance for KDP optics with conical mitigation contours processed by various paths intervals. Overall, the optical transmittance witnesses a moderate decline with the increase of path interval for spiral-milled surfaces. For tool marks with path interval of 10 μm, the corresponding spiral-milled surfaces possess the largest transmittance (T = 90.75%), which is very close the measured one of original fly-cut KDP surface (T = 90.95%). The similar transmittance values mean that the spiral-milling processes can be preferred in the practical engineering repair of KDP optics. And it can be found that about 0.4% transmittance loss for tool marks with 30 μm path interval (T = 90.56%) could be caused, which is obviously detrimental to the fluence outcome of the high-power laser system. While for layer-milled tool

Optical Materials EXPRESS

marks, as shown in Fig. 14, the measured transmittance (T = 90.72%) is quite close to that for tool marks with 15 μm path interval. This result is in accord with the simulation results as shown in Fig. 11. that the light intensification induced by layer-milled tool marks is at the middle of the I_{Rmax} induced by spiral-milled tool marks with various path intervals.

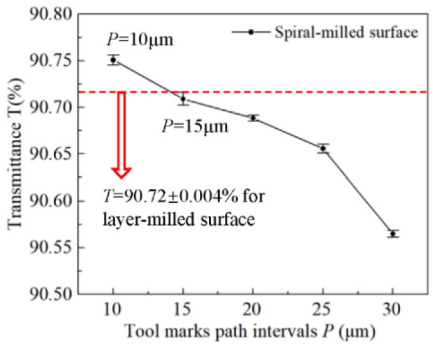

Fig. 14. Experimentally measured optical transmittance (T) of repaired KDP surfaces by layer-milling and spiral milling processes. The error bar is the standard deviation of the measured data.

The measured laser-induced damage thresholds (LIDTs) for KDP optics with different tool marks are exhibited in Fig. 15. It is shown that original fly-cut KDP surfaces possess a maximum LIDT up to 74.3 J/cm^2, while spiral-milled surfaces with 10 μm path intervals have a very close value as 72.1 J/cm^2. This means spiral-milling processes can produce a laser-friendly surface which has a similar laser damage resistance comparable to fly-cut surfaces [6], and tool marks with a path interval of 10 μm are strongly suggested for the future engineering repair of KDP optics. While with the increase of path interval, the LIDTs present a decreasing trend and the value for spiral-milled surface with 30 μm path interval is only 34.6 J/cm^2, indicating the tool marks with bigger path intervals have an inverse effect on the laser damage resistance and thus should be seriously considered before practical application in actual repair process.

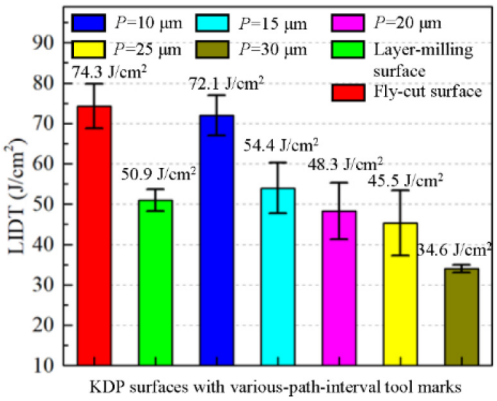

Fig. 15. The measured laser-induced damage threshold (LIDT) of repaired KDP surfaces with different types of tool marks.

Figure 16 exhibits the laser damage morphologies on KDP surfaces repaired by layer-milling process and spiral-milling path with path interval of 10 μm, respectively. It is clear to see that crack-type damage occurred on the layer-milled surface while shell-type damage took place on the spiral-milled surface. The higher LIDT for the spiral-milled surface (P = 10 μm) is responsible

Optical Materials EXPRESS

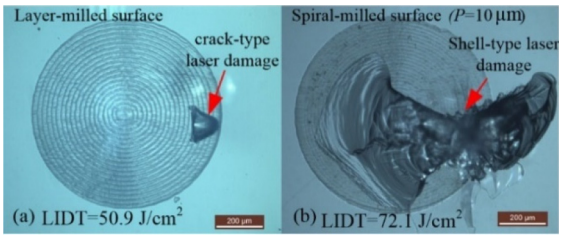

Fig. 16. Morphologies of micro-milled KDP surfaces when laser damage took place: (a) repaired surface by the layer-milling path; (b) repaired surface by the spiral-milling path with path intervals of 10 μm. The applied laser fluences are 50.9 J/cm^2 and 72.1 J/cm^2, respectively.

for this phenomenon because the shell-type damage morphology is often accompanied by higher laser fluence [7]. From the perspective of LIDT, the value for layer-milled surfaces (50.9 J/cm^2) is only below that for spiral-milled tool marks with path intervals of 10 μm and 15 μm. This scenario is quite different from the traditional concept where people always believe that the layer-milling process is not as good as spiral-milling for improving the laser damage resistance of repaired KDP optics. It is found for the first time that whether the spiral-milling is better than layer-milling or not for the optical performance of repaired KDP optics is dependent on the path interval used in the spiral-milling process. Therefore, based on the advantages of layer-milling and spiral-milling process, a new approach can be put forward to improve the efficiency and effectiveness of the repairing process. Considering the higher efficiency of removing material, the layer-milling can be adopted as rough milling to fabricate the predesigned mitigation contours quickly. Then, the spiral-milling can be utilized as fine-finish milling to produce a smooth surface with slight residual tool marks.

6. Conclusion

In this paper, the influence of residual tool marks on the light field intensity modulation inside micro-milled KDP optics and laser damage resistance was investigated theoretically and experimentally. The strategy for calculating the light intensity modulation induced by tool marks on complex 3D contours is demonstrated clearly. The experimental results verified the simulation results well under the same machining parameters. The main conclusions can be summarized as follows:

(1) A 3D surface formation model was developed to simulate the morphologies of repair contours processed by micro ball-end milling. The residual tool marks profiles on repaired surfaces can be accurately predicted.

(2) By adopting the predicted tool marks profiles, a light intensification model based on the finite element method was proposed to calculate the light intensity modulation inside micro-milled KDP optics with different tool marks. It is found the residual height of tool marks can result in strong diffraction effect inside KDP optics, causing higher light intensification.

(3) It reveals for the first time that in terms of improving the laser damage resistance of KDP optics, the spiral-milling process is not always better than layer-milling process. Whether the spiral-milling is better than layer-milling or not depends on the path interval used in the spiral-milling process. Only the spiral-milled tool marks with path intervals from 10~15 μm can have a better effect than layer-milled tool marks.

Optical Materials EXPRESS

(4) An optimized repair process flow is recommended for the practical engineering repair of KDP optics in ICF facilities. The layer-milling process can be adopted as rough-finish milling to fabricate the predesigned mitigation contours quickly. Then, the spiral-milling can be utilized as fine-finish milling to produce more slight residual tool marks, improving the laser damage resistance of KDP optics.

Funding

National Natural Science Foundation of China (51705105, 51775147); Science Challenge Project (TZ2016006-0503-01); CAST Innovation Foundation (2018QNRC001); China Postdoctoral Science Foundation (2017M621260, 2018T110288); Heilongjiang Provincial Postdoctoral Science Foundation (LBH-Z17090); Fundamental Research Funds for the Central Universities (HIT.NSRIF.2019053); State Key Laboratory of Robotics and System (SKLRS201718A, SKLRS201803B).

Acknowledgments

The first author also highly appreciates the support from the China Scholarship Council.

Disclosures

The authors declare that there are no conflicts of interest related to this article.

References

1. E. I. Moses and W. R. Meier, "Preparing for ignition experiments on the National Ignition Facility," Fusion Eng. Des. **83**(7-9), 997–1000 (2008).
2. D. Wang, T. Li, S. Wang, J. Wang, C. Shen, J. Ding, W. Li, P. Huang, and C. Lu, "Characteristics of nonlinear optical absorption and refraction for KDP and DKDP crystals," Opt. Mater. Express **7**(2), 533–541 (2017).
3. J. Stolz Christopher, "The National Ignition Facility: the path to a carbon-free energy future," Philos. Trans. R. Soc., A **370**(1973), 4115–4129 (2012).
4. Z. Zhang, H. Wang, X. Quan, G. Pei, M. Tian, T. Liu, K. Long, P. Li, and Y. Rong, "Optomechanical analysis and performance optimization of large-aperture KDP frequency converter," Opt. Laser Technol. **109**, 633–642 (2019).
5. S. Zhang, H. Zhang, and W. Zong, "Modeling and simulation on the effect of tool rake angle in diamond turning of KDP crystal," J. Mater. Process. Technol. **273**, 116259 (2019).
6. J. Cheng, M. Chen, W. Liao, H. Wang, J. Wang, Y. Xiao, and M. Li, "Influence of surface cracks on laser-induced damage resistance of brittle KH_2PO_4 crystal," Opt. Express **22**(23), 28740–28755 (2014).
7. Z. Liu, F. Geng, Y. Li, J. Cheng, H. Yang, Y. Zheng, J. Wang, and Q. Xu, "Study of morphological feature and mechanism of potassium dihydrogen phosphate surface damage under a 351 nm nanosecond laser," Appl. Opt. **57**(35), 10334–10341 (2018).
8. Y. Chen, H. Gao, X. Wang, D. Guo, and Z. Liu, "Laser Induced Damage of Potassium Dihydrogen Phosphate (KDP) Optical Crystal Machined by Water Dissolution Ultra-Precision Polishing Method," Materials **11**(3), 419 (2018).
9. X. Li, B. Liu, C. Yan, C. Liu, and X. Ju, "Structures of retired components and KDP crystals irradiated by high fluence using synchrotron μ-XRF and μ-XRD," Opt. Mater. Express **9**(2), 845–859 (2019).
10. X. Cai, X. Lin, G. Li, J. Lu, Z. Hu, and G. Zheng, "Rapid growth and properties of large-aperture 98%-deuterated DKDP crystals," High Power Laser Sci. Eng. **7**, e46 (2019).
11. W. Gao, J. Ji, C. Wang, L. Wang, Q. Fan, K. Sun, F. Ji, and M. Xu, "Mitigation of subsurface damage in potassium dihydrogen phosphate (KDP) crystals with a novel abrasive-free jet process," Opt. Mater. Express **8**(9), 2625–2635 (2018).
12. P. Geraghty, W. Carr, V. Draggoo, R. Hackel, C. Mailhiot, and M. Norton, "Surface damage growth mitigation on KDP/DKDP optics using single-crystal diamond micro-machining ball end mill contouring," Proc. SPIE **6403**, 64030Q (2007)..
13. L. W. Hrubesh, R. M. Brusasco, W. Grundler, M. A. Norton, E. E. Donohue, W. A. Molander, S. L. Thompson, S. R. Strodtbeck, P. K. Whitman, M. D. Shirk, P. J. Wegner, M. C. Nostrand, and A. K. Burnham, "Methods for mitigating growth of laser-initiated surface damage on DKDP optics at 351 nm," Proc. SPIE **4932**, 180 (2003)..
14. Q. Liu, J. Cheng, Y. Xiao, H. Yang, and M. Chen, "Effect of milling modes on surface integrity of KDP crystal processed by micro ball-end milling," Proc. CIRP **71**, 260–266 (2018).
15. Y. Xiao, M. Chen, Y. Yang, and J. Cheng, "Research on the critical condition of Brittle-Ductile Transition about Micro-Milling of KDP crystal and experimental verification," Int. J. Precis. Eng. Man. **16**(2), 351–359 (2015).
16. N. Chen, L. Li, J. Wu, J. Qian, N. He, and D. Reynaerts, "Research on the ploughing force in micro milling of soft-brittle crystals," Int. J. Mech. Sci. **155**, 315–322 (2019).

Optical Materials EXPRESS

17. H. Yang, J. Cheng, M. Chen, J. Wang, Z. Liu, C. An, Y. Zheng, K. Hu, and Q. Liu, "Optimization of morphological parameters for mitigation pits on rear KDP surface: experiments and numerical modeling," Opt. Express **25**(15), 18332–18345 (2017).
18. J. Cheng, H. Yang, Q. Liu, M. Chen, W. Ma, J. Tan, C. An, and Z. Liu, "Development of optimal mitigation contours and their machining flow by micro-milling to improve the laser damage resistance of KDP crystal," Proc. SPIE **10447**, 57 (2017)..
19. Y. Cai, Z. Liu, Z. Shi, Q. Song, and Y. Wan, "Residual surface topology modeling and simulation analysis for micro-machined nozzle," Int. J. Precis. Eng. Man. **16**(1), 157–162 (2015).
20. J. Chen, Y. Huang, and M. Chen, "A study of the surface scallop generating mechanism in the ball-end milling process," Int. J. Mach. Tool Manu. **45**(9), 1077–1084 (2005).
21. B. Corral, J. Vivancos Calvet, and A. Domínguez Fernández, "Surface topography in ball-end milling processes as a function of feed per tooth and radial depth of cut," Int. J. Mach. Tool Manu. **53**(1), 151–159 (2012).
22. F. Peng, J. Wu, Z. Fang, S. Yuan, R. Yan, and Q. Bai, "Modeling and controlling of surface micro-topography feature in micro-ball-end milling," Int. J. Adv. Manuf. Technol. **67**(9-12), 2657–2670 (2013).
23. M. Li, J. Huang, X. Liu, J. Wang, and L. Jia, "Research on surface morphology of the ruled surface in five-axis flank milling," Int. J. Adv. Manuf. Technol. **94**(5-8), 1655–1664 (2018).
24. W. Chen, L. Zheng, W. Xie, K. Yang, and D. Huo, "Modelling and experimental investigation on textured surface generation in vibration-assisted micro-milling," J. Mater. Process. Technol. **266**, 339–350 (2019).
25. W. Chen, W. Xie, D. Huo, and K. Yang, "A novel 3D surface generation model for micro milling based on homogeneous matrix transformation and dynamic regenerative effect," Int. J. Mech. Sci. **144**, 146–157 (2018).
26. Y. Cai, Z. Liu, Z. Shi, Q. Song, and Y. Wan, "Optimum end milling tool path and machining parameters for micro Laval nozzle manufacturing," Proc. Inst. Mech. Eng., Part B **231**(10), 1703–1712 (2017).
27. Z. Zhu, X. Zhou, D. Luo, and Q. Liu, "Development of pseudo-random diamond turning method for fabricating freeform optics with scattering homogenization," Opt. Express **21**(23), 28469–28482 (2013).
28. Z. Zhu, S. To, and S. Zhang, "Active control of residual tool marks for freeform optics functionalization by novel biaxial servo assisted fly cutting," Appl. Opt. **54**(25), 7656–7662 (2015).
29. N. L. Boling, M. D. Crisp, and G. Dubé, "Laser Induced Surface Damage," Appl. Opt. **12**(4), 650–660 (1973).
30. J. Cheng, M. Chen, K. Kafka, D. Austin, J. Wang, Y. Xiao, and E. Chowdhury, "Determination of ultra-short laser induced damage threshold of KH_2PO_4 crystal: Numerical calculation and experimental verification," AIP Adv. **6**(3), 035221 (2016).
31. D. Zhu, Y. Li, Q. Zhang, J. Wang, and Q. Xu, "Laser induced damage due to scratches in the surface of nonlinear optical crystals KH_2PO_4 (KDP)," J. Eur. Opt. Soc-Rapid. **13**(1), 33 (2017).
32. J. Cheng, M. Chen, W. Liao, H. Wang, Y. Xiao, and M. Li, "Fabrication of spherical mitigation pit on KH_2PO_4 crystal by micro-milling and modeling of its induced light intensification," Opt. Express **21**(14), 16799–16813 (2013).
33. N. Chen, M. Chen, C. Wu, and X. Pei, "Cutting surface quality analysis in micro ball end-milling of KDP crystal considering size effect and minimum undeformed chip thickness," Precis. Eng. **50**, 410–420 (2017).
34. Q. Liu, J. Cheng, Y. Xiao, M. Chen, H. Yang, and J. Wang, "Effect of tool inclination on surface quality of KDP crystal processed by micro ball-end milling," Int. J. Adv. Manuf. Technol. **99**(9-12), 2777–2788 (2018).
35. N. Chen, M. Chen, Y. Guo, and X. Wang, "Effect of cutting parameters on surface quality in ductile cutting of KDP crystal using self-developed micro PCD ball end mill," Int. J. Adv. Manuf. Technol. **78**(1-4), 221–229 (2015).
36. Q. Liu, J. Cheng, Z. Liao, H. Yang, L. Zhao, and M. Chen, "Incident laser modulation by tool marks on micro-milled KDP crystal surface: Numerical simulation and experimental verification," Opt. Laser Technol. **119**, 105610 (2019).
37. M. Q. Li, "Study on influence of KDP crystal ultra-precision fly-cutting micro/nano-topography on its laser induced damage threshold," *Harbin: Harbin Institute of Technology* 41–47 (2013).
38. J. Cheng, Y. Xiao, Q. Liu, H. Yang, L. Zhao, M. Chen, J. Tan, W. Liao, J. Chen, and X. Yuan, "Effect of surface scallop tool marks generated in micro-milling repairing process on the optical performance of potassium dihydrogen phosphate crystal," Mater. Des. **157**, 447–456 (2018).
39. W. Jiang, M. Chen, M. Li, and K. Chen, "Study of the near-field modulation property of microwaviness on a KH_2PO_4 crystal surface," Chin. Phys. B **19**(6), 064203 (2010).
40. C. L. He and W. J. Zong, "Diffraction effect and its elimination method for diamond-turned optics," Opt. Express **27**(2), 1326–1344 (2019).
41. Q. Zhang, Q. Zhao, S. To, B. Guo, and W. Zhai, "Diamond wheel wear mechanism and its impact on the surface generation in parallel diamond grinding of RB-SiC/Si," Diamond Relat. Mater. **74**, 16–23 (2017).